Journal of Environmental Chemical Engineering 8 (2020) 104184

Contents lists available at ScienceDirect

Journal of Environmental Chemical Engineering

journal homepage: www.elsevier.com/locate/jece

Complexation mechanisms in arsenic and phosphorus adsorption onto iron-coated cork granulates

Ariana M.A. Pintor*, Bárbara R.C. Vieira, Cátia C. Brandão, Rui A.R. Boaventura, Cidália M.S. Botelho*

Laboratory of Separation and Reaction Engineering – Laboratory of Catalysis and Materials (LSRE-LCM), Departamento de Engenharia Química, Faculdade de Engenharia da Universidade do Porto, Rua Dr. Roberto Frias, 4200-465 Porto, Portugal

ARTICLE INFO

Editor: Yunho Lee

Keywords:
Complexation
Adsorption
Arsenic
Phosphate
Potentiometric titration
Surface charge

ABSTRACT

The complexation mechanisms involved in As(III), As(V) and P(V) adsorption by iron-coated cork granulates, at environmentally relevant conditions (C_i = 1 mg L^{-1} and presence of background electrolyte), are analysed in this work.

Adsorption kinetics and potentiometric titration data were acquired for the three species. It was found that the adsorption rate was faster at 0.01 mol L^{-1} than 0.1 mol L^{-1} IS. Kinetic data were well fitted by the pseudo-first-order model for As(V) and P(V) and by the pseudo-second-order and Elovich models for As(III).

The adsorbed amount at equilibrium and the adsorption edges showed that As(III) adsorption was favoured at lower IS (especially at low pH), while As(V) and P(V) were favoured at higher IS (especially at higher pH). It is likely that all three species are adsorbed by inner-sphere complexation, although uptake of neutral As(III) is more affected by ion pair formation. In the case of As(V) and P(V), higher electrolyte uptake led to a decrease of the repulsive interactions and increased adsorption.

The surface charge estimation and modelling using a quasi-Gaussian Sips distribution function of affinity constants confirmed the likelihood of inner-sphere complexation. It is presumed that phosphate competes with hydroxyl ions for adsorption sites, leading to pH increase due to OH^- release in ligand exchange reactions.

It was verified that most adsorption mechanisms responsible for uptake onto pure iron oxides are also applicable in iron-coated adsorbents.

1. Introduction

Arsenic is a metalloid whose presence in water is a major risk for public health worldwide [1]. It is classified as a class 1 carcinogen and its concentration in drinking water is limited to a maximum allowed value of 10 µg L^{-1} as recommended by the World Health Organization [2]. For this reason, water sources contaminated with arsenic need proper treatment before they become suitable for human consumption. One of the most successful methodologies applied for this purpose is adsorption onto iron-based materials [3]. A study on the development of iron-coated cork granulates for As uptake has been recently reported [4].

Phosphorus belongs to the same group of the periodic table as arsenic, and consequently shares with it many chemical properties. In fact, most arsenic toxicity can be attributed to its substitution of phosphorus in biological processes [3,5]. In their pentavalent states, both As and P are usually present as oxyanions surrounded by four oxygen atoms, one double-bonded and three single-bonded, in a tetrahedral structure [6,7], and their acidity constants are very similar [7,8]. However, the environmental behaviour of As and P differ due to their different sensitivity to redox conditions. While phosphorus is rarely found in an oxidation state other than P(V), arsenic can be found as As (III) in anoxic systems, such as groundwaters [1,6]. Chemical and biological interactions that determine toxicity, adsorption, and complexation, to name a few, can vary greatly whether As is found in the trivalent or the pentavalent form.

The interaction of As and P with iron oxide surfaces is of great importance, as it influences their environmental fate and determines

Abbreviations: FAAS, flame atomic absorption spectrometry; GFAAS, graphite furnace atomic absorption spectrometry; ICG, iron-coated cork granulates; IS, ionic strength; pH_{PZC}, point of zero charge; RCG, raw cork granulates; SE, standard error; S/L, solid/liquid ratio

* Corresponding authors.
E-mail addresses: ampintor@fe.up.pt (A.M.A. Pintor), brdc.vieira@gmail.com (B.R.C. Vieira), catiabrandao@fe.up.pt (C.C. Brandão), bventura@fe.up.pt (R.A.R. Boaventura), cbotelho@fe.up.pt (C.M.S. Botelho).

https://doi.org/10.1016/j.jece.2020.104184
Received 20 February 2020; Received in revised form 9 June 2020; Accepted 13 June 2020
Available online 15 June 2020
2213-3437/

Nomenclature

Symbols

a	Initial adsorption rate (mg g^{-1} h^{-1})
b	Reciprocal of the surface coverage when the adsorption rate is 1/e of its initial value (g mg^{-1})
C_f	Final concentration of the adsorbate (mg L^{-1})
C_H	Proton concentration (mol L^{-1})
C_i	Initial concentration of the adsorbate (mg L^{-1})
k_1	Pseudo-first-order kinetic constant (h^{-1})
k_2	Pseudo-second-order kinetic constant (g mg^{-1} h^{-1})
$K'_{j,H}$	Median value for the affinity distribution of protons to the binding group j
m	Mass of adsorbent (g)
$m_{H,j}$	Width of the peak in the Sips distribution
N	Number of points
q	Adsorbed amount (mg g^{-1})
q_e	Adsorbed amount at equilibrium (mg g^{-1})
q_{exp}	Experimental value of q (mg g^{-1})
Q_H	Adsorbed amount of protons (mmol g^{-1})
$Q_{max,j}$	Overall charge of the binding group j (mmol g^{-1})
q_{pred}	Predicted value of q (mg g^{-1})
r^2	Correlation coefficient
s^2	Variance of the model
t	Time (h)
T	Temperature (ºC)
V	Solution volume (L)
w	Number of parameters estimated by the model

the effectiveness of iron-based adsorbents in their removal from water. Most researchers agree that, since Fe oxides and hydroxides show high selectivity towards the pnictogens, these are likely to be adsorbed through specific inner-sphere complexation [9–11]. Nevertheless, electrostatic interactions may play a role in As attraction to iron surface groups, given the reported variations of adsorption capacity with pH according to speciation [4,12–14]. Similarly, phosphate may be electrostatically bound to iron oxyhydroxides at acidic pH [8].

A possible methodology for the identification of the main complexation mechanism responsible for an adsorbate's uptake is the study of its adsorption behaviour with varying ionic strength. When the adsorbed amount decreases with the presence of other ions, this indicates that adsorption occurs on non-specific sites, i.e., by outer-sphere complexation [15,16]. On the other hand, if the adsorption capacity is unaffected or positively affected by ionic strength, it is likely that the interactions are specific, corresponding to the formation of inner-sphere complexes [17–19]. Furthermore, inner-sphere complexation may also alter the surface charge of the adsorbent, leading, in the case of anion uptake, to the lowering of the point of zero charge (pH_{PZC}) [20].

Previous research has shown that iron-coated cork granulates are promising adsorbents for As(III) and As(V) removal from water. Although this material's maximum adsorption capacity is lower than that of pure iron oxide materials, it proves to be a suitable carrier for practical applications, since iron oxides are usually present in powder form, and as such are not adequate for adsorption column configurations [4]. At the same time, it is believed that a better understanding of complexation interactions is crucial for the design of effective treatment systems that are robust enough to withstand a wide range of environmental conditions and possible competitive effects between adsorbed species. In a previous study by the authors on antimony uptake by iron-coated cork granulates the effect of pH, ionic strength and surface charge on both Sb(III) and Sb(V) adsorption at environmentally relevant concentrations was assessed, and related to inner- and outer-sphere complexation mechanisms [21]. The present work aims to apply the same methodology in order to identify the type of complexation mechanisms involved in As(III), As(V) and P(V) uptake by the same adsorbents. Although several studies can be found on As and P complexation on iron oxides [10,19,20,22–30], to the authors' knowledge, there are few papers [31] on the description of these mechanisms in iron-coated materials. It is, therefore, important to obtain novel data and verify if the same theoretical explanations for As and P uptake hold for low-cost, environmentally friendly adsorbents, which will be more widely used in practical applications such as water treatment technologies.

2. Materials and methods

2.1. Materials

The raw cork granulates (RCG) used for this study were supplied by Corticeira Amorim, S.G.P.S. in the particle size of 0.8–1.0 mm. The iron-coated cork granulates (ICG) were produced from these materials following a coating procedure with iron oxyhydroxide precipitates from a $FeCl_3$ 0.05 mol L^{-1} solution neutralized at pH 7, as optimized in a previous study [4]. RCG were contacted with this suspension in a 20 g L^{-1} solid/liquid (S/L) ratio, in a rotating shaker (SB3, Stuart) at 20 rpm during 24 h at a controlled temperature of 20.0 ± 0.5 °C. They were then washed with distilled water for five short cycles and left to dry in an oven (60 ± 1 °C) overnight. The iron content (determined after acid digestion of the coated solids) was on average 24 ± 2 mg g^{-1}.

Arsenic and phosphorus solutions were prepared from commercial stock solutions: 1000 ± 3 mg L^{-1} of As(III) in 4% HNO_3 (SCP Science), 1000 ± 3 mg L^{-1} of As(V) in 2–5 % HNO_3 (Chem-Lab), and 10,000 ± 40 mg L^{-1} of P as H_3PO_4 in 2–5 % HNO_3 (Chem-Lab).

2.2. Analytical methods

2.2.1. Arsenic

Total arsenic concentrations were determined by graphite furnace atomic absorption spectrometry (GFAAS) in the range $3-50\ \mu g\ L^{-1}$ after proper dilution of the samples. The equipment for this purpose was a GBC GF3000, SensAA Dual spectrometer, operating at a wavelength of 197.3 nm, lamp current of 5.0 mA, slit width of 1.0 nm and with a 70 s heating program culminating with the reading at 2400 °C vaporization temperature.

2.2.2. Iron

Total dissolved iron was determined by flame atomic absorption spectrometry (FAAS) in the range $0.1-5\ mg\ L^{-1}$, using a spectrometer GBC 932 Plus operating at a wavelength of 248.3 nm, lamp current of 5.0 mA and slit width of 0.2 nm, under air-acetylene flame.

2.2.3. Phosphorus

Dissolved phosphate was determined as phosphorus content by the colorimetric method with ascorbic acid (Standard Methods 4500-P E [32]), in the range $0-1\ mg\ L^{-1}$ of P. A combined reagent consisting of H_2SO_4 (95 %, AnalaR NORMAPUR, VWR), potassium antimony tartrate (> 99 %, ACRÓS Organics), ammonium molybdate (ACS, Reag. Ph. Eur, AnalaR NORMAPUR, VWR) and ascorbic acid (AnalaR NORMAPUR, VWR) was used to develop molybdenum blue colour whose intensity was measured at 880 nm in a UV–vis spectrophotometer (UV-6300PC, VWR).

2.3. Adsorption tests

2.3.1. Adsorption kinetics with varying ionic strength

The adsorption kinetics at environmentally relevant concentrations (1 mg L^{-1}) of As(III), As(V) and P(V) were assessed by performing batch adsorption assays with varying contact time (15 min (when necessary), 30 min, 1 h, 2 h, 4 h, 8 h, 16 h, 24 h, and 40 h and 48 h (when necessary)). For all species, a series of assays was performed with an ionic strength (IS) of 0.01 mol L^{-1}, and another with 0.1 mol L^{-1} IS, with NaCl as the background electrolyte, except for As(III) and As(V) where KNO_3 was used due to chloride interference with As measurement by GFAAS. The initial pH was adjusted to 9 for As(III) and 3 for As(V) and P(V), according to previous optimization [4], using NaOH and HNO_3 solutions.

The batch adsorption assays were carried out by contacting 45 mL of a 1 mg L^{-1} solution of As(III), As(V) or P(V) with 2.5 g L^{-1} ICG in 50 mL tubes for the determined time in a rotating shaker at 20 rpm, at a controlled temperature of 20.0 ± 0.5 °C. After contact, the aqueous samples were filtered through 0.45 µm acetate cellulose filters and analysed for As by GFAAS, P by the colorimetric method, and Fe by FAAS. The adsorbed amount (q, mg g^{-1}) was calculated by the following equation:

$$q = \frac{V\,(C_i - C_f)}{m} \quad (1)$$

Where V is the solution volume (L), C_i and C_f are the initial and final concentrations of the adsorbate (mg L^{-1}), respectively, and m is the mass of adsorbent (g).

2.3.2. Potentiometric titrations and acquisition of the adsorption edges

Potentiometric titrations of ICG surface at ionic strengths of 0.01 and 0.1 mol L^{-1} were carried out in the presence of As(III), As(V) or P(V). For each titration point, 45 mL of a neutral 1 mg L^{-1} solution of As(III), As(V) or P(V) with added 0.1 mol L^{-1} HCl (0.1 to 0.5 mL) or 0.1 mol L^{-1} NaOH (0.1 to 0.5 mL) was contacted with 2.5 g L^{-1} of ICG for 24 h in a rotating shaker at 20 rpm and controlled temperature of 20.0 ± 0.5 °C. Neutral and basic solutions were bubbled with N_2 before addition of the adsorbent in order to minimize the dissolution of CO_2 and the interference of carbonates. Blank assays were carried out in order to determine the baseline behaviour in the absence of ICG. After the predetermined contact time, samples were filtered, the final pH was measured and As or P were analysed by GFAAS or colorimetry, as appropriate. The adsorbed amount was calculated by Eq. (1).

All adsorption assays were carried out in duplicate and the average values were used as final results. The standard uncertainty was estimated taking into account the propagation of uncertainties in measurement and the absolute deviation between replicates and the average.

3. Results and discussion

3.1. Adsorption kinetics

The adsorption kinetics obtained at different ionic strengths, in environmentally relevant concentrations (1 mg L^{-1} As(III), As(V) or P(V)) and the respective best fitting models are presented in Fig. 1.

Three adsorption kinetic models were used to describe the adsorption data for each case, namely the pseudo-first-order model (Eq. (2)) [33], the pseudo-second-order model (Eq. (3)) [34] and the Elovich model (Eq. (4)) [35]:

$$q = q_e(1 - e^{-k_1 t}) \quad (2)$$

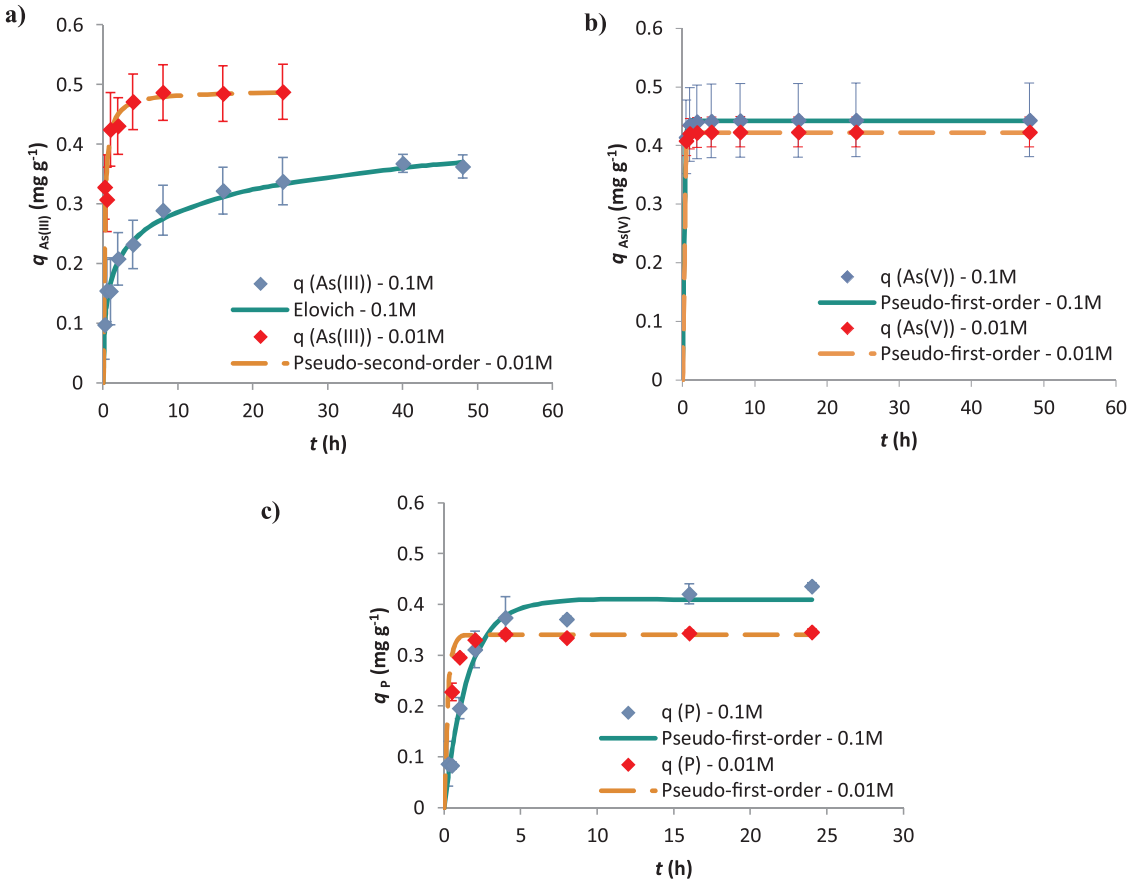

Fig. 1. Adsorption kinetics of a) As(III) (pH 9), b) As(V) (pH 3) and c) P(V) (pH 3), at 0.01 and 0.1 mol L^{-1} IS (C_i = 1 mg L^{-1}; S/L = 2.5 g L^{-1}; T = 20.0 ± 0.5 °C), along with the best fitting model curve for each dataset (error bars: standard uncertainty).

$$q = \frac{k_2 q_e^2 t}{1 + k_2 q_e t} \quad (3)$$

$$q = \frac{1}{b}\ln(1 + abt) \quad (4)$$

Where q (mg g^{-1}) is the adsorbed amount at time t (h), q_e (mg g^{-1}) is the adsorbed amount at equilibrium, k_1 (h^{-1}) is the pseudo-first-order kinetic constant, k_2 (g mg^{-1} h^{-1}) is the pseudo-second-order kinetic constant, a (mg g^{-1} h^{-1}) is the initial adsorption rate, and b (g mg^{-1}) is the reciprocal of the surface coverage when the adsorption rate is 1/e of its initial value.

The fitting of the models to the experimental data was carried out by non-linear fitting using software *CurveExpert Professional* v. 2.6.4. The fitting results for all models are presented in Table 1.

Fig. 1 clearly shows that the adsorbed amount is negatively affected by ionic strength in the case of As(III), but positively influenced for As (V) and P(V). Moreover, the adsorption rate is faster for all adsorbates at the ionic strength of 0.01 mol L^{-1}, with the difference being more pronounced for As(III) and P(V), for which the kinetic constants vary by an order of magnitude (Table 1). This effect on the uptake kinetics had already been observed for the adsorption of Sb(III) and Sb(V) on ICG [21].

For both pentavalent pnictogens, kinetics were well described by the pseudo-first-order model. This model is indicative of fast, monolayer physisorption, and this is likely to occur since the initial adsorbate concentration is low and thus so is the surface coverage of the adsorbent. At pH 3, ICG surface is positively charged [4], and therefore attracts the negatively charged oxyanions of As(V) and P(V), which are in the form of $H_2AsO_4^-$ [36] and $H_2PO_4^-$ [37], respectively. However, the equilibrium adsorbed amount for both As(V) and P(V) increased with ionic strength, which is indicative of chemical covalent linkage and inner-sphere complexation mechanisms [19,26].

Meanwhile, adsorption of As(III) presents slower kinetics, better described by the pseudo-second-order or Elovich equations, suggesting the occurrence of chemisorption and heterogeneous, multilayer binding [38,39]. Nonetheless, the equilibrium adsorbed amount was higher for the lower level of ionic strength, implying that outer-sphere complexation mechanisms were at play for which the electrolyte ions competed with arsenite anions [19].

Because some of the models presented similar r^2 and SE, an F-test was also carried out to compare the model fits for each scenario, according to the equation:

$$F = \frac{{s_A}^2}{{s_B}^2} \quad (5)$$

Where ${s_A}^2$ is the variance of model A and ${s_B}^2$ is the variance of model B, each one calculated by:

$$s^2 = \frac{\sum_{i=1}^{N}(q_{exp} - q_{pred})^2}{N - w} \quad (6)$$

Where q_{exp} is the experimental value of q, q_{pred} the predicted value of q according to the model fit, N is the number of points and w the number of estimated parameters in the model. The F-value as calculated by Eq. (5) was then compared to the critical F-value for a confidence level of 95 %. It was found that for As(III), 0.01 mol L^{-1} IS, As(V), both IS scenarios, and P(V), 0.1 mol L^{-1} IS, the model fits did not present a significant difference; only the Elovich model for As(III), 0.1 mol L^{-1} IS and the pseudo-first-order model for P(V), 0.01 mol L^{-1} IS were significantly better than the other models. This could explain the existence of both physical and chemical adsorption mechanisms occurring in most of these cases, since different kinetic models are suitable for most of the scenarios.

A slight desorption of iron was observed in almost all of the kinetic studies, with a maximum observed for As(V) at pH 3 and 0.1 mol L^{-1} IS, after 48 h contact, of 2.8 ± 0.1 mg L^{-1}. However, this did not seem to have any influence on the adsorbed amounts, since, for instance, for the same species at 0.01 mol L^{-1} IS both the As adsorbed amount at equilibrium and the desorbed iron amount were lower.

Further studies on the adsorption edges of all three kinds of anions under study aimed to clarify their uptake mechanisms.

3.2. Adsorption edges

The variation of the adsorption edges of As(III), As(V) and P(V) on ICG with ionic strength was assessed at environmentally relevant concentrations (C_i = 1 mg L^{-1}). The results are depicted in Fig. 2.

The results corroborate the conclusions drawn from the equilibrium adsorbed amounts reported for the kinetic studies. Fig. 2a shows that As (III) uptake is favoured at lower ionic strength, in particular at low pH, while Figs. 2b and c show the inverse for As(V) and P(V), that is, that adsorption is increased at higher ionic strength, especially at higher pH.

Desorption of iron in these studies was also slight, always below 3 mg L^{-1}, and without any observable effect on the adsorbed amounts. For all scenarios it had a tendency to be higher at more acidic (< 3) and more basic (> 10) pH.

Comparing these and the kinetic results with a previous study on As uptake by ICG [4], it can be concluded that both As(III) and As(V) trends of variation with pH and time differ between low and high surface coverage. At an initial concentration of 25 mg L^{-1}, As(III)

Table 1
Model parameters obtained for the fitting of pseudo-first-order, pseudo-second-order and Elovich models to the adsorption kinetics data of As(III), As(V) and P(V) (C_i = 1 mg L^{-1}; S/L = 2.5 g L^{-1}; T = 20.0 ± 0.5 °C) at different ionic strengths.

		As(III), pH 9		As(V), pH 3		P(V), pH 3	
IS (mol L^{-1})		0.01	0.1	0.01	0.1	0.01	0.1
Pseudo-first-order model (Eq. (2))	q_e (mg g^{-1})	0.46 ± 0.02	0.33 ± 0.02	0.4227 ± 0.0003	0.4419 ± 0.0009	0.341 ± 0.002	0.41 ± 0.01
	k_1 (h^{-1})	3.2 ± 0.7	0.6 ± 0.2	6.7 ± 0.3	5.5 ± 0.2	4.3 ± 0.2	0.64 ± 0.08
	r2	0.667	0.803	0.966	0.956	0.986	0.973
	SE	0.05	0.05	0.001	0.002	0.005	0.03
Pseudo-second-order model (Eq. (3))	q_e (mg g^{-1})	0.49 ± 0.01	0.35 ± 0.02	0.4245 ± 0.0007	0.445 ± 0.001	0.352 ± 0.005	0.46 ± 0.02
	k_2 (g mg^{-1} h^{-1})	12 ± 3	2.5 ± 0.7	134 ± 17	68 ± 8	25 ± 4	1.7 ± 0.4
	r2	0.860	0.918	0.914	0.939	0.942	0.968
	SE	0.03	0.03	0.002	0.003	0.01	0.03
Elovich model (Eq. (4))	a (mg g^{-1} h^{-1})	(0.6 ± 1.1) × 10^3 (n.s.)	1.2 ± 0.2	n.c.	n.c.	(0.7 ± 3.5) × 10^5 (n.s.)	0.8 ± 0.4
	b (g mg^{-1})	25 ± 5	18.9 ± 0.8	n.c.	n.c.	50 ± 16	11 ± 2
	r2	0.826	0.987	n.c.	n.c.	0.636	0.915
	SE	0.03	0.01	n.c.	n.c.	0.03	0.05

n.s. – not significant; n.c. – non convergent.

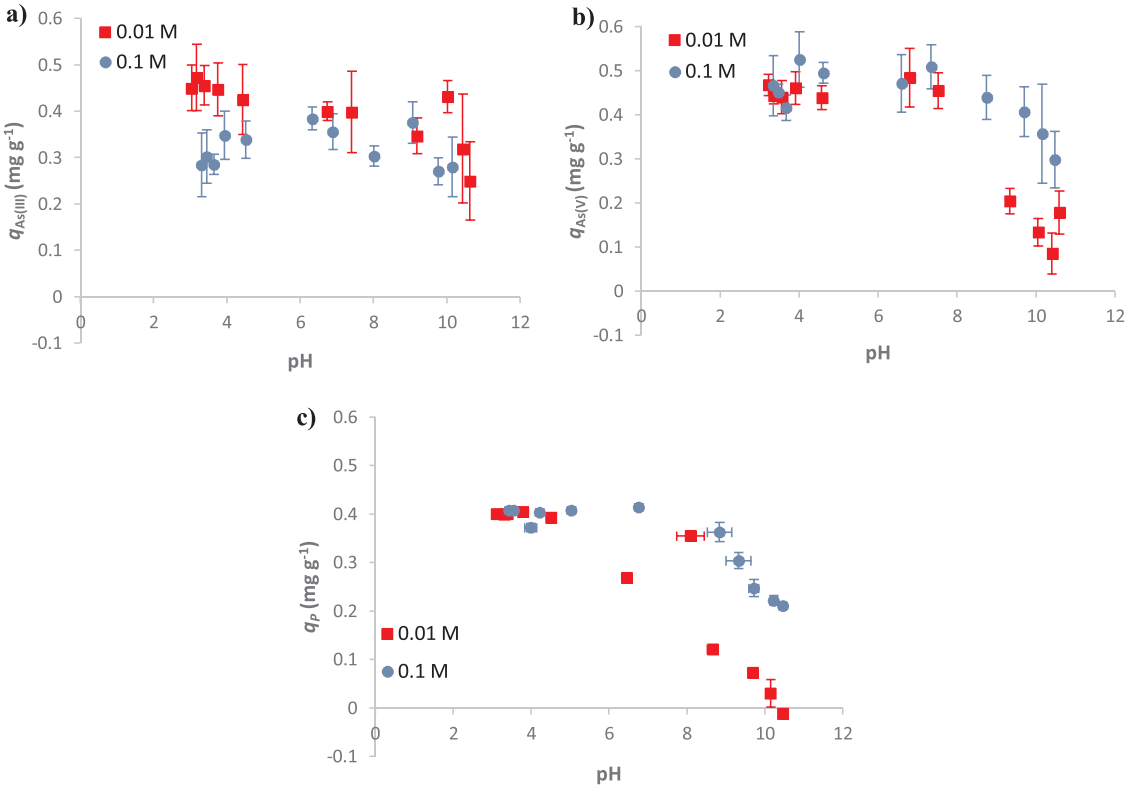

Fig. 2. Adsorption edges of a) As(III), b) As(V) and c) P(V), at 0.01 and 0.1 mol L^{-1} IS (C_i = 1 mg L^{-1}; S/L = 2.5 g L^{-1}; T = 20.0 ± 0.5 °C) (error bars: standard uncertainty).

adsorption was faster than As(V) [4], while the opposite was observed for an initial loading of 1 mg L^{-1} As (Fig.1, Table 1). At higher surface coverage, uptake of As(III) increased with pH with a maximum at pH 9; however, by Fig. 2a, the same does not apply at lower surface coverage, when the adsorbed amount varies little with pH and even seems to decrease with increasing pH for 0.01 mol L^{-1} IS values. In a similar fashion, at higher surface coverage pH 2 was identified as providing the highest As(V) adsorption [4], which decreases steadily with increasing pH; at lower surface coverage, however, As(V) uptake is maximum for a wider pH range (3–7), starting to decrease only for values above 8. These results are in accordance with previous studies of As(III) and As (V) adsorption kinetics and envelopes on ferrihydrite [40].

It has been stated that As(III) adsorbs more weakly than As(V) onto iron oxides at low pH [7,20,41], and in fact it is in the range 3–5 that a higher influence of IS is observed for the trivalent oxidation state (Fig. 2a), suggesting the occurrence of outer-sphere complexation. However, electrostatic attraction between As(III) and the surface is unlikely since in this range of acidic pH, it is present in the neutral form, H_3AsO_3 or $As(OH)_3$ [36]. Still, as the surface is positively charged, as it is below the pH_{PZC} (estimated as 6 for ICG [21]), attraction of NO_3^-, the ion of the electrolyte, may occur, as it is negatively charged, and its uptake may lead to a coverage of surface sites, hindering As(III) access for specific binding. Uptake of As(III) is likely to occur as inner-sphere complexes in the remaining sites, by ligand exchange with OH^-, as it has been proposed by several authors to be the main binding mechanism [20,26]. Binding of oxyanions is often assumed to occur at singly-coordinated Fe surface groups (≡FeOH, or, in their protonated/deprotonated forms, $\equiv FeOH_2^{1/2+}$ and $\equiv FeOH^{1/2-}$ [42]), which are dominant at the ferrihydrite surface [43]. Stachowicz et al. [44] maintain that As(III) adsorption may occur in its neutral form as a monodentate or bidentate complex, depending if it binds with one or two surface groups:

$$1 \equiv FeOH(s) + As(OH)_3(aq) \rightleftharpoons \equiv FeOAs(OH)_2(ads) + H_2O(l) \quad (7)$$

$$2 \equiv FeOH(s) + As(OH)_3(aq) \rightleftharpoons \equiv Fe_2O_2As(OH)(ads) + 2H_2O(l) \quad (8)$$

These authors also demonstrated that bidentate binding is usually predominant, with monodentate binding only becoming relevant at lower pH. Since monodentate complexes are tendentially weaker than bidentate bonds, if they are more affected by the formation of outer-sphere complexes with electrolyte ions, this influence may contribute to the higher dependence of As(III) adsorbed amount with ionic strength at low pH.

The binding of As(V), on the other hand, has often been modelled on iron oxides based on the formation of three types of complexes: protonated bidentate, non-protonated bidentate, and protonated monodentate [44]:

$$2 \equiv FeOH(s) + 3H^+(aq) + AsO_4^{3-}(aq) \rightleftharpoons \equiv Fe_2O_2AsOOH(ads) + 2H_2O(l) \quad (9)$$

$$2 \equiv FeOH(s) + 2H^+(aq) + AsO_4^{3-}(aq) \rightleftharpoons \equiv Fe_2O_2AsO_2(ads) + 2H_2O(l) \quad (10)$$

$$1 \equiv FeOH(s) + 2H^+(aq) + AsO_4^{3-}(aq) \rightleftharpoons \equiv FeOAsO_2OH(ads) + H_2O(l) \quad (11)$$

Surface complexation modelling carried out on crystalline goethite surfaces usually indicates bidentate binding as the predominant form of complexation for As(V) [19,44,45], but for amorphous ferrihydrite, some authors successfully consider monodentate binding as the main adsorption mechanism [25,46,47]. Most studies, however, maintain that it is difficult to distinguish monodentate and bidentate binding based on the available experimental data [20,44,48–50]. Nevertheless, the results presented in Fig. 2b are closely in accordance with predictions made for As(V) adsorption on goethite by Antelo et al. [19], with a decrease in adsorbed amount starting at neutral pH, and slightly sharper for lower IS. The increased uptake caused by higher IS in the alkaline pH range, especially above the pH_{PZC}, is probably due to a decrease of the repulsive interaction between the surface and the anion,

produced by the presence of electrolyte [19,51].

A few authors also suggest that surface precipitation of ferric arsenate may occur as an adsorption mechanism for As(V) at higher As loadings [18,25,50]. This phenomenon was found to be particularly relevant at acidic pH, due to the larger extent of Fe dissolution [25], and therefore may be responsible for the marked increase of As(V) uptake with decrease of pH previously observed at higher surface coverage [4].

Regarding phosphorus, the trend of phosphate adsorption variation with pH and IS is also in accordance with previous results reported for iron oxides, with constant uptake at acidic pH and a decrease with increasing pH, sharper than that observed for As(V) [19,22,27,28]. There is, however, less agreement over the mode of phosphate binding than arsenate binding in the literature. Overall, six types of complexes, monodentate and bidentate with different degrees of protonation, have been proposed as possible contributors to phosphate binding on singly coordinated surface groups [52]:

$$1 \equiv FeOH(s) + H^+(aq) + PO_4^{3-}(aq) \rightleftharpoons \equiv FeOPO_3OH(ads) + H_2O(l) \quad (12)$$

$$1 \equiv FeOH(s) + 2H^+(aq) + PO_4^{3-}(aq) \rightleftharpoons \equiv FeOPO_2OH(ads) + H_2O(l) \quad (13)$$

$$1 \equiv FeOH(s) + 3H^+(aq) + PO_4^{3-}(aq) \rightleftharpoons \equiv FeOPO(OH)_2(ads) + H_2O(l) \quad (14)$$

$$2 \equiv FeOH(s) + 2H^+(aq) + PO_4^{3-}(aq) \rightleftharpoons \equiv Fe_2O_2PO_2(ads) + 2H_2O(l) \quad (15)$$

$$2 \equiv FeOH(s) + 3H^+(aq) + PO_4^{3-}(aq) \rightleftharpoons \equiv Fe_2O_2POOH(ads) + 2H_2O(l) \quad (16)$$

$$2 \equiv FeOH(s) + 4H^+(aq) + PO_4^{3-}(aq) \rightleftharpoons \equiv Fe_2O_2P(OH)_2(ads) + 2H_2O(l) \quad (17)$$

Studies on phosphate complexation on goethite have proposed with equal success models based on the three monodentate complexes (Eq. (12)–(14)) [28,53,54], on two bidentate complexes (mostly Eqs. (15) and (16)) [19,55], or on a combination of both monodentate and bidentate complexes [23,52]. Studies on ferrihydrite have also proposed similar configurations of bidentate complexation [22,24] or monodentate complexation [27]. If a combination of bidentate and monodentate binding is present, it is likely that bidentate binding is favoured at low pH [19,22,23,51], which helps to explain stronger adsorption in this range.

The effect of ionic strength on P(V) adsorption at higher pH may also be caused, as for As(V), by a reduction of the electrostatic repulsion between surface and anion through electrolyte uptake. In particular, this is found to be more pronounced for phosphate because P has been found to be more sensitive to pH and ionic strength changes [19] and has more affinity for ion pair formation with Na [54].

3.3. Surface charge

The surface charge was estimated by the adsorbed amount of protons Q_H (mmol g^{-1}), which was modelled using a bimodal distribution of affinity constants, following a quasi-Gaussian Sips distribution function [56] with a local Langmuir-Freundlich isotherm. As a simplification, two types of sites are considered: acidic sites with low intrinsic constant and basic sites with high intrinsic constant.

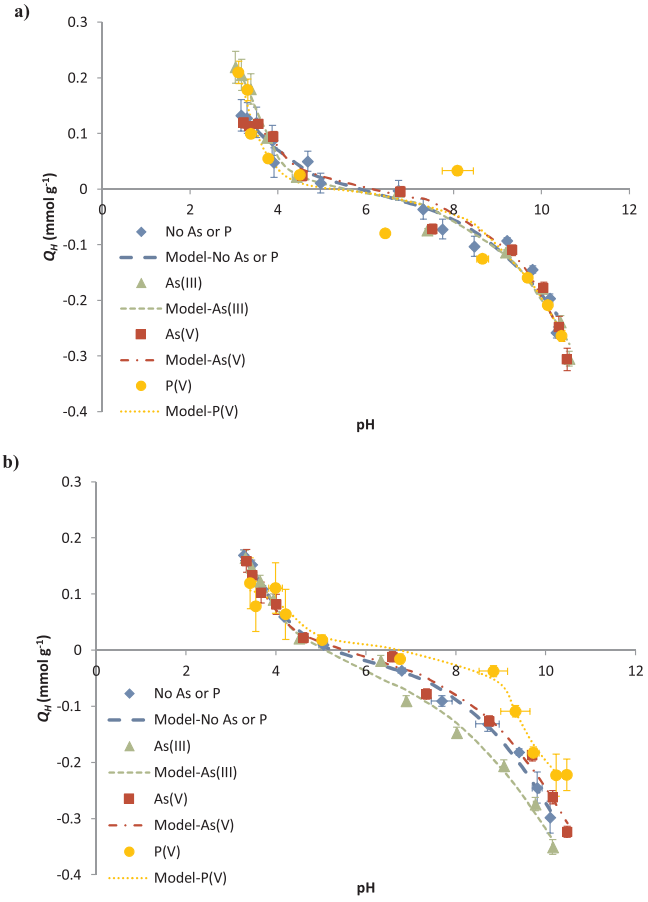

Fig. 3. Experimental data and Sips distributions of surface charge of ICG in the absence and presence of As(III), As(V) and P(V) (C_i = 1 mg L^{-1}; S/L = 2.5 g L^{-1}; T = 20.0 ± 0.5 °C) in a) 0.01 mol L^{-1} IS and b) 0.1 mol L^{-1} IS (error bars: standard uncertainty).

$$Q_H = Q_{max,1}\frac{(K'_{1,H}C_H)^{m_{H,1}}}{1+(K'_{1,H}C_H)^{m_{H,1}}} - Q_{max,2}\left(1-\frac{(K'_{2,H}C_H)^{m_{H,2}}}{1+(K'_{2,H}C_H)^{m_{H,2}}}\right) \quad (18)$$

Where $Q_{max,j}$ is the overall charge of the binding group j (mmol g^{-1}), $K'_{j,H}$ is the median value for the affinity distribution of protons to the binding group j, C_H is the proton concentration (mol L^{-1}), and $m_{H,j}$ is the width of the peak in the Sips distribution ($0 < m_{H,j} < 1$).

The model was fitted using the methodology presented by Vilar et al. [57]. The obtained parameters are shown in Table 2 and the results for surface charge, along with the model curves, are presented in Fig. 3. For comparison purposes, the surface charge and models without

Table 2
Parameters obtained in the fitting of the Sips distribution function for different ionic strength conditions and in the presence of the different adsorbed species.

IS (mol L^{-1})	Adsorbed species (C_i = 1 mg L^{-1})	log$K'_{1,H}$	$Q_{max,1}$ (mmol g^{-1})	$m_{H,1}$	log$K'_{2,H}$	$Q_{max,2}$ (mmol g^{-1})	$m_{H,2}$	r^2
0.01	As(III)	3.4	0.32	1.0	11.0	0.66	0.4	0.989
	As(V)	4.1	0.14	1.0	11.0	0.71	0.4	0.984
	P(V)	2.3	1.47	0.9	11.0	0.68	0.4	0.936
0.1	As(III)	3.6	0.27	0.8	11.0	0.90	0.3	0.993
	As(V)	2.9	0.47	0.6	11.0	0.76	0.3	0.992
	P(V)	4.4	0.12	1.0	9.4	0.25	1.0	0.986

As or P are presented as previously determined [4,21].

At an ionic strength of 0.01 mol L^{-1}, the charge distributions obtained in the presence of the species under study are all very similar to the original surface charge distribution of ICG (Fig. 3a). The only noticeable difference is a slight decrease of the pH_{PZC} and an increase in positive surface charge at acidic pH for As(III) and P(V). Decrease of the isoelectric point (IEP) or pH_{PZC} has been reported to occur in the formation of inner-sphere complexes [19,28,58,59]. However, this decrease was also found to be dependent on the surface loading of the adsorbate [28,59]. In this study, the initial concentration of 1 mg L^{-1} As or P corresponds to 13.3 μmol L^{-1} As or 32.3 μmol L^{-1} P. These lead to very low surface loadings that correspond, at most, to the ratios of $10-20$ mmol-As mol-Fe^{-1} or $30-40$ mmol-P mol-Fe^{-1}. Naturally, their effect on the adsorbent's surface charge is also low.

Nevertheless, at the higher ionic strength of 0.1 mol L^{-1} a significant increase on the pH_{PZC} can be found when P(V) is adsorbed (Fig. 3b). This is contrary to the aforementioned studies that reported, for instance, a decrease in IEP after P adsorption on goethite [28]. However, in the quoted study, the original pH_{PZC} was high (about 8.8), as it is expected for pure iron oxides, while for ICG, as the iron coating is not homogeneous and both iron and organic groups interact with protons, the pH_{PZC} falls in the neutral to acidic range, around 5–6 [4,21]. In the present study, the pH_{PZC} becomes more alkaline after phosphate is adsorbed but it is shifted towards more neutral values, close to 7. It is possible that phosphate is acting as a buffer in these conditions. Another possibility is the occurrence of competition between phosphate and hydroxyl (OH-) at the iron oxide surface, leading to OH- release by ligand exchange with the phosphate ions [38,46]. This would cause a rapid increase in pH and overall increased H^+ consumption in the alkaline range, as depicted in Fig. 3b.

At higher IS, ion pair formation with Na and K on the iron oxide surface may also be enhanced [19,22,54]. For the pentavalent species, which are negatively charged in the neutral to alkaline pH range, it may bear no effect and even enhance their uptake. For the neutral As(III), while a higher amount of positively charged ions bound at the surface may not interfere with As uptake (Fig. 2a), they may increase the uptake of negatively charged OH^-, explaining the slight increase in negative charge in this pH range observed in Fig. 3b.

4. Conclusions

This study allowed to gain some insight on the complexation mechanisms of As(III), As(V) and P(V) on iron-coated cork granulates at environmentally relevant conditions.

The adsorption kinetics suggests a combination of physisorption mechanism, described by a pseudo-first-order model, and chemisorption mechanism, described by a pseudo-second-order model, with more prevalence of the former for the pentavalent species As(V) and P(V), while of the latter for As(III). However, the adsorption edges at different ionic strengths indicated otherwise, with As(III) adsorption being favoured at lower ionic strength and As(V) and P(V) uptake enhanced at higher ionic strength. The results indicate that both physical and chemical adsorption mechanisms are involved in the uptake of all these species in environmentally relevant conditions.

Given the unlikelihood of outer-sphere complexation of As(III), it is proposed that it is bound by inner-sphere complexation, but that monodentate binding may be affected by outer-sphere complexation of electrolyte anions. As(V) and P(V) are also likely to form inner-sphere rather than outer-sphere complexes at the iron oxide surface, possibly by a combination of both monodentate and bidentate binding; for As (V), ferric arsenate precipitation may also be present, which would be detrimental for future adsorbent regeneration and reuse.

Surface charge estimation by potentiometric titration confirmed the likelihood of inner-sphere complex formation for all three species, along with outer-sphere complexation and ion pair formation with electrolyte ions. Phosphate may act as a buffer in these conditions and suffer competition with hydroxyl ions, leading to increased pH and H^+ consumption in the alkaline range.

The application of previous literature on As and P adsorption onto iron oxides to interpret their uptake mechanisms onto iron-coated cork granulates confirms that the iron coating is responsible for adsorption. At the same time, this is one of the first studies that verifies that complexation mechanisms on pure iron oxides and iron-coated adsorbents are very similar.

This can be especially useful since conclusions drawn for iron-coated adsorbents help to determine the sensitivity of As(III), As(V) and P(V) adsorption to treatment conditions, thereby aiding in the optimization of their removal in water treatment systems.

CRediT authorship contribution statement

Ariana M.A. Pintor: Conceptualization, Methodology, Formal analysis, Writing - original draft, Visualization. **Bárbara R.C. Vieira:** Investigation, Validation, Visualization. **Cátia C. Brandão:** Investigation, Validation, Visualization. **Rui A.R. Boaventura:** Writing - review & editing, Funding acquisition. **Cidália M.S. Botelho:** Resources, Writing - review & editing, Funding acquisition.

Declaration of Competing Interest

None.

Acknowledgements

Funding: This work is a result of: Project "AIProcMat@N2020 - Advanced Industrial Processes and Materials for a Sustainable Northern Region of Portugal 2020", with the reference NORTE-01-0145-FEDER-000006, supported by Norte Portugal Regional Operational Programme (NORTE 2020), under the Portugal 2020 Partnership Agreement, through the European Regional Development Fund (ERDF); Associate Laboratory LSRE-LCM - UID/EQU/50020/2019 - funded by national funds through FCT/MCTES (PIDDAC). A. Pintor acknowledges her postdoctoral fellowship [SFRH/BPD/117680/2016] and her Junior Researcher contract [CEECIND/01485/2017] by FCT.

The authors kindly acknowledge Corticeira Amorim, S.G.P.S. for providing the cork granulates for this study.

References

[1] W. Ali, A. Rasool, M. Junaid, H. Zhang, A comprehensive review on current status, mechanism, and possible sources of arsenic contamination in groundwater: a global perspective with prominence of Pakistan scenario, Environ. Geochem. Health 41 (2019) 737–760, https://doi.org/10.1007/s10653-018-0169-x.
[2] Guidelines for Drinking-water Quality, World Health Organization, 2011.
[3] D.E. Giles, M. Mohapatra, T.B. Issa, S. Anand, P. Singh, Iron and aluminium based adsorption strategies for removing arsenic from water, J. Environ. Manag. 92 (2011) 3011–3022, https://doi.org/10.1016/j.jenvman.2011.07.018.
[4] A.M.A. Pintor, B.R.C. Vieira, S.C.R. Santos, R.A.R. Boaventura, C.M.S. Botelho, Arsenate and arsenite adsorption onto iron-coated cork granulates, Sci. Total Environ. 642 (2018) 1075–1089, https://doi.org/10.1016/j.scitotenv.2018.06.170.
[5] P. Ghosh, B. Rathinasabapathi, M. Teplitski, L.Q. Ma, Bacterial ability in AsIII oxidation and AsV reduction: relation to arsenic tolerance, P uptake, and siderophore production, Chemosphere 138 (2015) 995–1000, https://doi.org/10.1016/j.chemosphere.2014.12.046.
[6] D.G. Strawn, Review of interactions between phosphorus and arsenic in soils from four case studies, Geochem. Trans. 19 (2018) 10, https://doi.org/10.1186/s12932-018-0055-6.
[7] P. Qi, T. Pichler, Competitive adsorption of As(III), As(V), Sb(III) and Sb(V) onto ferrihydrite in multi-component systems: implications for mobility and distribution, J. Hazard. Mater. 330 (2017) 142–148, https://doi.org/10.1016/j.jhazmat.2017.02.016.
[8] M.I. Rivas-Pérez, R. Paradelo-Núñez, C.J. Nóvoa-Muñoz, M. Arias-Estévez, J.M. Fernández-Sanjurjo, E. Álvarez-Rodríguez, A. Núñez-Delgado, As(V) and P competitive sorption on soils, by-products and waste materials, Int. J. Environ. Res. Public Health 12 (2015) 15706–15715, https://doi.org/10.3390/ijerph121215016.
[9] M.A. Inam, R. Khan, D.R. Park, B.A. Ali, A. Uddin, I.T. Yeom, Influence of pH and contaminant redox form on the competitive removal of arsenic and antimony from aqueous media by coagulation, Miner. 8 (2018) 574, https://doi.org/10.3390/

min8120574.
[10] N.Y. Dzade, N.H. de Leeuw, Density functional theory characterization of the structures of H3AsO3 and H3AsO4 adsorption complexes on ferrihydrite, Environ. Sci. Process. Impacts 20 (2018) 977–987, https://doi.org/10.1039/C7EM00608J.
[11] H. Zhang, M. Elskens, G. Chen, L. Chou, Phosphate adsorption on hydrous ferric oxide (HFO) at different salinities and pHs, Chemosphere 225 (2019) 352–359, https://doi.org/10.1016/j.chemosphere.2019.03.068.
[12] E. Pehlivan, H.T. Tran, W.K.I. Ouédraogo, C. Schmidt, D. Zachmann, M. Bahadir, Sugarcane bagasse treated with hydrous ferric oxide as a potential adsorbent for the removal of As(V) from aqueous solutions, Food Chem. 138 (2013) 133–138, https://doi.org/10.1016/j.foodchem.2012.09.110.
[13] J. Han, H.-M. Ro, Interpreting competitive adsorption of arsenate and phosphate on nanosized iron (hydr)oxides: effects of pH and surface loading, Environ. Sci. Pollut. Res. 25 (2018) 28572–28582, https://doi.org/10.1007/s11356-018-2897-y.
[14] L. Lin, W. Qiu, D. Wang, Q. Huang, Z. Song, H.W. Chau, Arsenic removal in aqueous solution by a novel Fe-Mn modified biochar composite: characterization and mechanism, Ecotoxicol. Environ. Saf. 144 (2017) 514–521, https://doi.org/10.1016/j.ecoenv.2017.06.063.
[15] Y. Miao, F. Han, B. Pan, Y. Niu, G. Nie, L. Lv, Antimony(V) removal from water by hydrated ferric oxides supported by calcite sand and polymeric anion exchanger, J. Environ. Sci. China (China) 26 (2014) 307–314, https://doi.org/10.1016/S1001-0742(13)60418-0.
[16] Z. He, R. Liu, H. Liu, J. Qu, Adsorption of Sb(III) and Sb(V) on freshly prepared ferric hydroxide (FeOxHy), Environ. Eng. Sci. 32 (2014) 95–102, https://doi.org/10.1089/ees.2014.0155.
[17] R.-J. Deng, C.-S. Jin, B.-Z. Ren, B.-L. Hou, S.A. Hursthouse, The potential for the treatment of antimony-containing wastewater by iron-based adsorbents, Water 9 (2017) 794, https://doi.org/10.3390/w9100794.
[18] B. Lan, Y. Wang, X. Wang, X. Zhou, Y. Kang, L. Li, Aqueous arsenic (As) and antimony (Sb) removal by potassium ferrate, Chem. Eng. J. 292 (2016) 389–397, https://doi.org/10.1016/j.cej.2016.02.019.
[19] J. Antelo, M. Avena, S. Fiol, R. López, F. Arce, Effects of pH and ionic strength on the adsorption of phosphate and arsenate at the goethite–water interface, J. Colloid Interface Sci. 285 (2005) 476–486, https://doi.org/10.1016/j.jcis.2004.12.032.
[20] A. Jain, K.P. Raven, R.H. Loeppert, Arsenite and arsenate adsorption on ferrihydrite: surface charge reduction and net OH- release stoichiometry, Environ. Sci. Technol. 33 (1999) 1179–1184, https://doi.org/10.1021/es980722e.
[21] A.M.A. Pintor, B.R.C. Vieira, R.A.R. Boaventura, C.M.S. Botelho, Removal of antimony from water by iron-coated cork granulates, Sep. Purif. Technol. 233 (2020) 116020, , https://doi.org/10.1016/j.seppur.2019.116020.
[22] J. Antelo, S. Fiol, C. Pérez, S. Mariño, F. Arce, D. Gondar, R. López, Analysis of phosphate adsorption onto ferrihydrite using the CD-MUSIC model, J. Colloid Interface Sci. 347 (2010) 112–119, https://doi.org/10.1016/j.jcis.2010.03.020.
[23] D.B. Abdala, P.A. Northrup, F.C. Vicentin, D.L. Sparks, Residence time and pH effects on the bonding configuration of orthophosphate surface complexes at the goethite/water interface as examined by Extended X-ray Absorption Fine Structure (EXAFS) spectroscopy, J. Colloid Interface Sci. 442 (2015) 15–21, https://doi.org/10.1016/j.jcis.2014.11.048.
[24] Y. Arai, D.L. Sparks, ATR–FTIR spectroscopic investigation on phosphate adsorption mechanisms at the ferrihydrite–Water interface, J. Colloid Interface Sci. 241 (2001) 317–326, https://doi.org/10.1006/jcis.2001.7773.
[25] X. Jiang, C. Peng, D. Fu, Z. Chen, L. Shen, Q. Li, T. Ouyang, Y. Wang, Removal of arsenate by ferrihydrite via surface complexation and surface precipitation, Appl. Surf. Sci. 353 (2015) 1087–1094, https://doi.org/10.1016/j.apsusc.2015.06.190.
[26] B.A. Manning, S.E. Fendorf, S. Goldberg, Surface structures and stability of arsenic (III) on goethite: spectroscopic evidence for inner-sphere complexes, Environ. Sci. Technol. 32 (1998) 2383–2388, https://doi.org/10.1021/es9802201.
[27] H.A. Mengistu, A. Tessema, M.B. Demlie, T.A. Abiye, O. Roeyset, Surface-complexation modelling for describing adsorption of phosphate on hydrous ferric oxide surface, Water Sa 41 (2015) 157–168, https://doi.org/10.4314/wsa.v41i1.19.
[28] N. Nilsson, L. Lövgren, S. Sjöberg, Phosphate complexation at the surface of goethite, Chem. Speciat. Bioavailab. 4 (1992) 121–130, https://doi.org/10.1080/09542299.1992.11083190.
[29] D. Yan, H.-J. Li, H.-Q. Cai, M. Wang, C.-C. Wang, H.-B. Yi, X.-B. Min, Microscopic insight into precipitation and adsorption of As(V) species by Fe-based materials in aqueous phase, Chemosphere 194 (2018) 117–124, https://doi.org/10.1016/j.chemosphere.2017.11.150.
[30] J. Han, H.-M. Ro, Characterizing preferential adsorption of phosphate on binary sorbents of goethite and maghaemite using in situ ATR-FTIR and 2D correlation spectroscopy, Sci. Rep. 9 (2019) 6130, https://doi.org/10.1038/s41598-019-42575-2.
[31] H. Pan, H. Hou, J. Chen, H. Li, L. Wang, Adsorption of arsenic on iron modified attapulgite (Fe/ATP): surface complexation model and DFT studies, Adsorpt. 24 (2018) 459–469, https://doi.org/10.1007/s10450-018-9959-9.
[32] A.D. Eaton, Standard Methods for the Examination of Water and Wastewater, American Public Health Association, Baltimore, Maryland, U.S.A, 2005.
[33] S.Y. Lagergren, Zur theorie der sogenannten adsorption gelöster stoffe, K. Sven. Vetensk. Handl. 24 (1898) 1–39.
[34] Y.S. Ho, Adsorption of Heavy Metals From Waste Streams by Peat, The University of Birmingham, Birmingham, U.K, 1995.
[35] M.J.D. Low, Kinetics of chemisorption of gases on solids, Chem. Rev. 60 (1960) 267–312, https://doi.org/10.1021/cr60205a003.
[36] G. Ungureanu, S. Santos, R. Boaventura, C. Botelho, Arsenic and antimony in water and wastewater: Overview of removal techniques with special reference to latest advances in adsorption, J. Environ. Manag. 151 (2015) 326–342, https://doi.org/10.1016/j.jenvman.2014.12.051.
[37] P. Loganathan, S. Vigneswaran, J. Kandasamy, N.S. Bolan, Removal and recovery of phosphate from water using sorption, Crit. Rev. Environ. Sci. Technol. 44 (2014) 847–907, https://doi.org/10.1080/10643389.2012.741311.
[38] Z. Ajmal, A. Muhmood, M. Usman, S. Kizito, J. Lu, R. Dong, S. Wu, Phosphate removal from aqueous solution using iron oxides: adsorption, desorption and regeneration characteristics, J. Colloid Interface Sci. 528 (2018) 145–155, https://doi.org/10.1016/j.jcis.2018.05.084.
[39] Z. Wang, C.C. Ainsworth, D.M. Friedrich, P.L. Gassman, A.G. Joly, Kinetics and mechanism of surface reaction of salicylate on alumina in colloidal aqueous suspension, Geochim. Cosmochim. Acta 64 (2000) 1159–1172, https://doi.org/10.1016/S0016-7037(99)00360-9.
[40] K.P. Raven, A. Jain, R.H. Loeppert, Arsenite and arsenate adsorption on ferrihydrite: kinetics, equilibrium, and adsorption envelopes, Environ. Sci. Technol. 32 (1998) 344–349, https://doi.org/10.1021/es970421p.
[41] Y. Deng, Y. Li, X. Li, Y. Sun, J. Ma, M. Lei, L. Weng, Influence of calcium and phosphate on pH dependency of arsenite and arsenate adsorption to goethite, Chemosphere 199 (2018) 617–624, https://doi.org/10.1016/j.chemosphere.2018.02.018.
[42] T. Hiemstra, W.H. Van Riemsdijk, A surface structural approach to ion adsorption: the charge distribution (CD) model, J. Colloid Interface Sci. 179 (1996) 488–508, https://doi.org/10.1006/jcis.1996.0242.
[43] T. Hiemstra, W.H. Van Riemsdijk, A surface structural model for ferrihydrite I: sites related to primary charge, molar mass, and mass density, Geochim. Cosmochim. Acta 73 (2009) 4423–4436, https://doi.org/10.1016/j.gca.2009.04.032.
[44] M. Stachowicz, T. Hiemstra, W.H. van Riemsdijk, Surface speciation of As(III) and As(V) in relation to charge distribution, J. Colloid Interface Sci. 302 (2006) 62–75, https://doi.org/10.1016/j.jcis.2006.06.030.
[45] S. Fendorf, M.J. Eick, P. Grossl, D.L. Sparks, Arsenate and chromate retention mechanisms on goethite, 1. Surface Structure, Environ. Sci. Technol. 31 (1997) 315–320, https://doi.org/10.1021/es950653t.
[46] R.L. Vaughan, B.E. Reed, Modeling As(V) removal by a iron oxide impregnated activated carbon using the surface complexation approach, Water Res. 39 (2005) 1005–1014, https://doi.org/10.1016/j.watres.2004.12.034.
[47] G.A. Waychunas, B.A. Rea, C.C. Fuller, J.A. Davis, Surface chemistry of ferrihydrite: part 1. EXAFS studies of the geometry of coprecipitated and adsorbed arsenate, Geochim. Cosmochim. Acta 57 (1993) 2251–2269, https://doi.org/10.1016/0016-7037(93)90567-G.
[48] X. Guo, Y. Du, F. Chen, H.-S. Park, Y. Xie, Mechanism of removal of arsenic by bead cellulose loaded with iron oxyhydroxide (β-FeOOH): EXAFS study, J. Colloid Interface Sci. 314 (2007) 427–433, https://doi.org/10.1016/j.jcis.2007.05.071.
[49] A. Manceau, The mechanism of anion adsorption on iron oxides: evidence for the bonding of arsenate tetrahedra on free Fe(O, OH)6 edges, Geochim. Cosmochim. Acta 59 (1995) 3647–3653, https://doi.org/10.1016/0016-7037(95)00275-5.
[50] R. Nagar, D. Sarkar, K.C. Makris, R. Datta, Effect of solution chemistry on arsenic sorption by Fe- and Al-based drinking-water treatment residuals, Chemosphere 78 (2010) 1028–1035, https://doi.org/10.1016/j.chemosphere.2009.11.034.
[51] T. Hiemstra, W.H. Van Riemsdijk, Surface structural ion adsorption modeling of competitive binding of oxyanions by metal (Hydr)oxides, J. Colloid Interface Sci. 210 (1999) 182–193, https://doi.org/10.1006/jcis.1998.5904.
[52] R. Rahnemaie, T. Hiemstra, W.H. van Riemsdijk, Geometry, Charge Distribution, and Surface Speciation of Phosphate on Goethite, Langmuir 23 (2007) 3680–3689, https://doi.org/10.1021/la062965n.
[53] P. Persson, N. Nilsson, S. Sjöberg, Structure and bonding of orthophosphate ions at the Iron oxide–Aqueous interface, J. Colloid Interface Sci. 177 (1996) 263–275, https://doi.org/10.1006/jcis.1996.0030.
[54] Y. Gao, A. Mucci, Acid base reactions, phosphate and arsenate complexation, and their competitive adsorption at the surface of goethite in 0.7 M NaCl solution, Geochim. Cosmochim. Acta 65 (2001) 2361–2378, https://doi.org/10.1016/S0016-7037(01)00589-0.
[55] C. Luengo, M. Brigante, J. Antelo, M. Avena, Kinetics of phosphate adsorption on goethite: comparing batch adsorption and ATR-IR measurements, J. Colloid Interface Sci. 300 (2006) 511–518, https://doi.org/10.1016/j.jcis.2006.04.015.
[56] R. Sips, On the Structure of a Catalyst Surface. II, J. Chem. Phys. 18 (1950) 1024–1026, https://doi.org/10.1063/1.1747848.
[57] V.J.P. Vilar, C.M.S. Botelho, R.A.R. Boaventura, Effect of Cu(II), Cd(II) and Zn(II) on Pb(II) biosorption by algae gelidium-derived materials, J. Hazard. Mater. 154 (2008) 711–720, https://doi.org/10.1016/j.jhazmat.2007.10.084.
[58] B.A. Manning, S. Goldberg, Modeling competitive adsorption of arsenate with phosphate and molybdate on oxide minerals, Soil Sci. Soc. Am. J. 60 (1996) 121–131, https://doi.org/10.2136/sssaj1996.03615995006000010020x.
[59] S. Goldberg, C.T. Johnston, Mechanisms of arsenic adsorption on amorphous oxides evaluated using macroscopic measurements, vibrational spectroscopy, and surface complexation modeling, J. Colloid Interface Sci. 234 (2001) 204–216, https://doi.org/10.1006/jcis.2000.7295.